Multiphoton dissociation of a diatomic molecule including the effects of the continuum

Robert Graham and Michael Höhnerbach
Fachbereich Physik, Universität Gesamthochschule Essen, D4300 Essen 1, Germany
(Received 11 October 1991)

The dissociation of a diatomic molecule via the electromagnetic excitation of its vibrations is analyzed by a direct solution of the Schrödinger equation in the energy representation of the uncoupled molecule fully including the effects of the continuum. Using a Morse potential, all dipole matrix elements are obtained analytically. We give exact results for the bound-continuum matrix elements and semiclassical results for the continuum-continuum matrix elements corrected for the diverging density of states near the dissociation energy. We compute dissociation probabilities and the form of the excited wave packets in the bound and the unbound subspaces of the uncoupled molecule. The influence of a smooth switch-on and switch-off of the electromagnetic field is also analyzed. Our results are compared with and interpreted by the help of a simple Poincaré map ("Morse map") derived in earlier work.

PACS number(s): 33.80.Rv, 03.65.Sq

I. INTRODUCTION

The multiphoton excitation or dissociation of molecules continues to be a field of great current interest both from the point of view of applications and also as a subject of fundamental research [1–7]. One theoretical aspect which has received much attention is the fact that in a classical description the systems considered are chaotic; i.e., the dynamics of the actual quantum systems are instances of "quantum chaos" (for a review, see [8]). A characteristic difficulty in the theoretical treatment of the quantized systems arises from the fact that the phase space is noncompact and the energy spectrum has a continuous component. In a preceding paper [7], henceforth referred to as I, we have analyzed in some detail quantum effects on the multiphoton excitation of the vibrations in a Morse potential by reducing, in a certain approximation, the classical dynamics and associated Schrödinger equation to a classical map ("Morse map" [4]) and its quantized version, respectively. The same method has been used in [9] for hydrogen and in [5] for general nonlinear oscillators including the Morse oscillator. In the description used in I, the influence of the continuous part of the molecular spectrum on the bound states, caused by the deexcitation from the continuum to the bound states, is taken into account only during a finite time T after the excitation into the continuum, where T is given by the characteristic period of vibration of the remaining bound part of the wave packet.

While the resulting description of the multiphoton-absorption process in terms of a quantum map is attractively simple, it is, of course, only an approximation, and it is therefore desirable to perform more detailed and numerically exact calculations controlling the results of the more simple but approximate approach. The value of the latter then, of course, does not disappear, but consists in providing simple qualitative and quantitative physical insights which allow us to interpret the results of the more exact but physically less transparent numerical calculations.

It is the purpose of the present paper to present a direct numerical solution of the Schrödinger equation of a harmonically driven Morse oscillator in the energy representation of the Morse Hamiltonian. Specifically, we wish to analyze the following experimentally realizable situation: Diatomic molecules are first preexcited in a well-defined vibrational state. Subsequently, they interact with a strong monochromatic field of an infrared laser. Afterward the occupation probability of their vibrational levels and their dissociation probability is analyzed.

In the theoretical analysis we aim to include fully the effects of the continuum on the bound subspace, taking into account all continuum-bound and continuum-continuum transitions via their exact and semiclassically approximated matrix elements, respectively. To our knowledge such a calculation has not been performed before for the Morse oscillator. Some preliminary results of this approach were used in I [dashed lines in Figs. 4(b), 5(b), and 6(b) of I] in order to check the reliability of the description based on the quantized Morse map.

For a one-dimensional model of hydrogen in a periodic external electromagnetic field, a calculation similar to the one we shall present here for the Morse oscillator, also taking continuum-continuum transitions into account, has been given by Susskind and Jensen [10]. In addition, these authors compared the use of different gauges (the $\mathbf{p}\cdot\mathbf{A}$ coupling versus the $\mathbf{d}\cdot\mathbf{E}$ coupling) and different representations (hydrogenic versus Sturmian basis functions).

Our work will be restricted to the $\mathbf{p}\cdot\mathbf{A}$ gauge arising naturally from the minimal coupling Hamiltonian of the electromagnetic field and to the use of molecular (i.e., Morse) basis functions. The Hamiltonian of our problem is given by

$$H=\frac{[P-eA(\tau)]^2}{2M}+V(r)\ ,$$
$$V(r)=D(1-e^{-\alpha(r-r_0)})^2\ , \tag{1.1}$$

where D is the dissociation energy, r_0 the nuclear dis-

tance at equilibrium, α^{-1} the range of the molecular potential, M the reduced mass, and e the effective charge interacting with the external field. The vector potential $A(\tau)$ of the externally applied electric field of amplitude F and frequency ω_0 is

$$A=\frac{1}{\omega_0}F\sin\omega_0\tau \ . \tag{1.2}$$

Scaling all variables according to $x=r-r_0$, $p=P/\sqrt{2DM}$, and $t=\Omega_0\tau$, with $\Omega_0=\alpha\sqrt{2D/M}$, and introducing the two dimensionless parameters $g=eF/2D\alpha$ and $\omega=\omega_0/\Omega_0$, the Hamiltonian is cast into the form

$$H(x,p)=\frac{[p-(g/\omega)\sin\omega t]^2}{2}+\frac{1}{2}(1-e^{-x})^2 \ . \tag{1.3}$$

Our aim is the solution of the Schrödinger equation

$$i\hbar\dot{\psi}(x,t)=H\left[x,\frac{\hbar}{i}\frac{\partial}{\partial x}\right]\psi(x,t) \ , \tag{1.4}$$

where $\hbar$ is dimensionless, in our present units, and stands for $\hbar\alpha/\sqrt{2DM}$.

In Sec. II we shall formulate the Schrödinger equation in the molecular basis and provide analytical expressions for all required matrix elements. In Sec. III we present and discuss our results.

II. REPRESENTATION IN THE MOLECULAR BASIS

A. Molecular basis

The molecular basis is defined by the eigenfunctions of the Hamiltonian of the free molecule,

$$H_0=-\frac{\hbar^2}{2}\frac{\partial^2}{\partial x^2}+\frac{1}{2}(1-e^{-x})^2 \ . \tag{2.1}$$

The discrete part of the spectrum of

$$H_0\phi_\nu=E_\nu\phi_\nu \tag{2.2}$$

is given by the eigenvalues

$$E_\nu=\tfrac{1}{2}-\tfrac{1}{2}[-\hbar(\nu+\tfrac{1}{2})+1]^2 \ , \quad 0\le\nu<1/\hbar-\tfrac{1}{2} \ , \tag{2.3}$$

with the normalized eigenfunctions [11]

$$\phi_\nu(x)=\left[\frac{2\beta_\nu\nu!}{\Gamma(2\beta_\nu+\nu+1)}\right]^{1/2}z^{\beta_\nu}e^{-z/2}L_\nu^{(2\beta_\nu)}(z) \ , \tag{2.4}$$

with

$$\begin{aligned}&\beta_\nu=1/\hbar-(\nu+\tfrac{1}{2}) \ ,\\ &z=2e^{-x}/\hbar \ .\end{aligned} \tag{2.5}$$

$L_\nu^{(\mu)}(z)$ is the generalized Laguerre polynomial [12].

The continuous part of the spectrum of

$$H_0\phi(\kappa)=E(\kappa)\phi(\kappa) \tag{2.6}$$

consists of all energies

$$E(\kappa)=\hbar^2\kappa^2/2+\tfrac{1}{2} \ , \tag{2.7}$$

with $-\infty<\kappa<+\infty$, $E(\kappa)\ge\frac{1}{2}$, and the functions

$$\phi(x,\kappa)=N(\kappa)z^{i\kappa}e^{-z/2}U(i\kappa+\tfrac{1}{2}-1/\hbar,1+2i\kappa,z) \ , \tag{2.8}$$

where $U(a,b,z)$ is one of Kummer's functions in the notation of [12] and $N(\kappa)$ is a normalization constant, which we choose as real. Because of the existence of the Kummer transformation

$$U(a,b,z)=z^{1-b}U(1+a-b,2-b,z) \ , \tag{2.9}$$

the function $\phi(x,\kappa)$ is then also real, and all linearly independent solutions are covered by taking $\kappa\ge0$. Normalizing the continuum wave functions by

$$\int_{-\infty}^{+\infty}dx\ \phi^*(x,\kappa)\phi(x,\kappa')=\delta(\kappa-\kappa') \ , \tag{2.10}$$

we have to fix [13,14]

$$N(\kappa)=\frac{\sqrt{\kappa\sinh(2\pi\kappa)}}{\pi}\left|\Gamma\left[\frac{1}{2}-\frac{1}{\hbar}+i\kappa\right]\right| \ . \tag{2.11}$$

Let us expand the wave function in the molecular basis

$$\psi(x,t)=\sum_{\nu=0}^{\nu_{\max}}a_\nu(t)\phi_\nu(x)+\int_0^\infty d\kappa\, a(\kappa,t)\phi(x,\kappa) \ , \tag{2.12}$$

where $\nu_{\max}=[\hbar^{-1}-\frac{1}{2}]$ is the integer part of $\hbar^{-1}-\frac{1}{2}$, and introduce the interaction picture

$$\begin{aligned}&a_\nu(t)=\tilde{a}_\nu(t)e^{-i(E_\nu/\hbar)t} \ ,\\ &a(\kappa,t)=\tilde{a}(\kappa,t)e^{-i(E(\kappa)/\hbar)t} \ .\end{aligned} \tag{2.13}$$

Furthermore, we introduce the gauge transformation

$$\tilde{a}(t)=b(t)\exp\left[-\frac{ig^2}{4\omega^2}\left[t-\frac{1}{2\omega}\sin2\omega t\right]\right] \ , \tag{2.14}$$

where $\tilde{a}$ stands for $\tilde{a}_\nu,\tilde{a}(\kappa)$ and b for $b_\nu,b(\kappa)$. The Schrödinger equation then takes the form

$$\begin{aligned}&i\hbar\dot{b}_\nu=\sum_{\mu=0}^{\nu_{\max}}V_{\nu\mu}(t)b_\mu+\int_0^\infty d\kappa\, V_\nu(\kappa,t)b(\kappa) \ ,\\ &i\hbar\dot{b}(\kappa)=\sum_{\mu=0}^{\nu_{\max}}V_\mu^*(\kappa,t)b_\mu+\int_0^\infty d\kappa'\, V(\kappa,\kappa',t)b(\kappa') \ ,\end{aligned} \tag{2.15}$$

with

$$V_{ab}(t)=-\frac{g}{\omega}(\sin\omega t)p_{ab}e^{i\omega_{ab}t} \ . \tag{2.16}$$

Here the indices a,b stand for ν,μ or κ,κ' for the discrete and continuous parts of the spectrum, respectively, $\omega_{ab}=(E_a-E_b)/\hbar$, and

$$\begin{aligned}&p_{ab}=i\omega_{ab}x_{ab} \ ,\\ &x_{ab}=\int_{-\infty}^{+\infty}dx\ \phi_a^*(x)x\phi_b(x)\end{aligned} \tag{2.17}$$

are the dipole matrix elements.

B. Matrix elements in the discrete subspace

The discrete matrix elements

$$x_{\nu\mu}=\int_{-\infty}^{+\infty}dx\ \phi_\nu^*(x)x\phi_\mu(x) \ , \tag{2.18}$$

for $\nu \neq \mu$, have been calculated in [15] as

$$x_{\nu\mu} = 2(-1)^{\nu+\mu+1} \frac{\sqrt{\beta_\nu \beta_\mu}}{\beta_\nu^2 - \beta_\mu^2} \left[\frac{\mu! \Gamma(2\beta_\mu + \mu + 1)}{\nu! \Gamma(2\beta_\nu + \nu + 1)} \right]^{1/2}, \quad \nu < \mu$$

$$x_{\mu\nu} = x_{\nu\mu} . \tag{2.19}$$

We note that the matrix elements for $\nu = \mu$ are not needed here as $\omega_{\nu\nu} x_{\nu\nu} = 0$.

C. Matrix elements between discrete and continuous subspace

The discrete-continuous matrix elements

$$x_\nu(\kappa) = \int_{-\infty}^{+\infty} dx \, \phi_\nu^*(x) x \phi(x,\kappa) \tag{2.20}$$

are evaluated in Appendix A as

$$x_\nu(\kappa) = \frac{(-1)^{\nu+1}}{\pi} |\Gamma(\tfrac{1}{2} - 1/\hbar + i\kappa)| \times \sqrt{2\nu! \beta_\nu \Gamma(2\beta_\nu + \nu + 1) \kappa \sinh 2\pi\kappa} \times \sum_{\lambda=0}^{\nu} \frac{|\Gamma(\beta_\nu + i\kappa + \lambda)|^2}{\lambda! \Gamma(1 + 2\beta_\nu + \lambda)} . \tag{2.21}$$

Using an identity proven in Appendix B, the finite sum in (2.21) can be evaluated, and we obtain the final expression

$$x_\nu(\kappa) = \frac{(-1)^{\nu+1}}{\pi} \frac{|\Gamma(\tfrac{1}{2} - 1/\hbar + i\kappa)|}{\beta_\nu^2 + \kappa^2} \times \left[\frac{2\beta_\nu \kappa \sinh 2\pi\kappa}{\nu! \Gamma(2\beta_\nu + \nu + 1)} \right]^{1/2} \times |\Gamma(\beta_\nu + i\kappa + \nu + 1)|^2 . \tag{2.22}$$

D. Matrix elements in semiclassical approximation

The matrix elements $p(\kappa,\kappa')$ in the continuous subspace are tedious to evaluate, even though it seems likely that analytical expressions may be obtained. Even so, the final expressions are likely not to be simple, and it is therefore of interest to obtain manageable closed-form expressions in an accurate approximation designed for highly excited states. This is the semiclassical approximation. Matrix elements of dynamical variables in the semiclassical approximation can be obtained from the Fourier transform by a standard method described, e.g., in [16]. We first consider the discrete subspace where the approximation can be controlled by a comparison with the results of Sec. II A. Then we shall apply the method to obtain the continuum-continuum matrix elements in the semiclassical approximation.

1. Bound supspace

The classical motion of the free molecule is described best in action angle variables I, Θ (see, e.g., I, Secs. II B and II C). For the motion of the momentum, we then find [see Eqs. (2.14) and (2.15) of I]

$$p(I,t) = \sum_{m=-\infty}^{\infty} p(I,\omega_m) e^{i\omega_m(I)t} , \tag{2.23}$$

with

$$p(I,\omega_m) = -i(1-I) \left[\frac{I}{2-I} \right]^{m/2} , \quad \omega_m(I) = m(1-I) . \tag{2.24}$$

Here I in the interval $0 \leq I < 1$ is the action variable

$$I = \frac{1}{2\hbar} \oint p \, dx , \tag{2.25}$$

of the bound motion. The following semiclassical expression for the matrix element $p_{\nu\mu}$ is derived in [16]:

$$p_{\nu+m,\nu} \approx p(I_\nu, \omega_m(I_\nu)) , \tag{2.26}$$

where, in the present application,

$$I_\nu = \hbar(\nu + \tfrac{1}{2}) = 1 - \hbar\beta_\nu , \quad \omega_m(I_\nu) = m[1 - \hbar(\nu + \tfrac{1}{2})] . \tag{2.27}$$

Here I_ν is the Bohr-Sommerfeld-quantized action variable. In the following we shall use a more symmetrical version of (2.26), namely,

$$p_{\nu\mu} \approx p\left[\frac{1}{2}(I_\nu + I_\mu), \omega_{\nu-\mu}\left[\frac{I_\nu + I_\mu}{2} \right] \right] . \tag{2.28}$$

From (2.27) we then obtain

$$p_{\nu\mu} \approx -i \left[1 - \hbar \left[\frac{\nu+\mu}{2} + \frac{1}{2} \right] \right] \times \left[\frac{\hbar(\nu+\mu)+1}{4 - \hbar(\nu+\mu+1)} \right]^{(\nu-\mu)/2} , \quad \nu > \mu$$

$$p_{\mu\nu} = p_{\nu\mu}^* , p_{\nu\nu} = 0 . \tag{2.29}$$

The derivation of the semiclassical matrix elements in [16] is based on the explicit assumption that the dependence on the quantum number ν is weak. This will be satisfied if the semiclassical expression for the coarse-grained (over an action scale $\sim\hbar$) density of states

$$\rho_\nu = \left[\hbar \frac{\partial H_0(I_\nu)}{\partial I_\nu} \right]^{-1} = \frac{1}{\hbar(1 - I_\nu)} \tag{2.30}$$

varies weakly with I_ν. Here $H_0(I) = I - \frac{1}{2}I^2$ is the molecular Hamiltonian as a function of the action variable. We see that ρ_ν diverges at the dissociation border $I_\nu \to 1$; i.e., the assumption for the validity of (2.26) or (2.28) breaks down, and we have to expect deviations between the semiclassical results (2.29) and the exact results (2.17) and (2.19) if either I_ν or I_μ approaches the dissociation border.

The divergence of the average density of states at the dissociation border leads to the vanishing of the normalization factor of the wave function (2.4) proportional to the inverse square root of ρ_ν,

$$\rho_\nu^{-1/2} \sim \sqrt{\beta_\nu} , \tag{2.31}$$

and the corresponding vanishing of the matrix element

$$x_{\nu\mu} = i\omega_{\nu\mu} p_{\nu\mu} \sim \rho_\nu^{-1/2} \rho_\mu^{-1/2} , \tag{2.32}$$

as can be seen in (2.19). Indeed, this is not correctly reproduced by our expression (2.29), which vanishes $\sim(\rho_\nu^{-1}+\rho_\mu^{-1})$. In order to correct for this defect, we shall multiply our semiclassical approximant by the factor

$$\frac{2\rho_\nu^{-1/2}\rho_\mu^{-1/2}}{(\rho_\nu^{-1}+\rho_\mu^{-1})} = \frac{2\rho_\nu^{1/2}\rho_\mu^{1/2}}{\rho_\nu+\rho_\mu} . \tag{2.33}$$

The same correction shall also be applied to continuum-continuum matrix elements determined below, to which the same reasoning applies, with the only difference that the average density of states in the present argument is there replaced by the true density of states. After multiplication with the factor (2.33), our semiclassical result for the bound-bound matrix elements becomes

$$p_{\nu\mu} \approx -i\hbar\sqrt{\beta_\nu\beta_\mu}\left[\frac{1-\hbar(\beta_\nu+\beta_\mu)/2}{1+\hbar(\beta_\nu+\beta_\mu)/2}\right]^{\nu-\mu} , \quad \nu>\mu$$
$$p_{\mu\nu} = p_{\nu\mu}^* , p_{\nu\nu} = 0 , \tag{2.34}$$

and $x_{\nu\mu} = i\omega_{\nu\mu} p_{\nu\mu}$.

Clearly, the semiclassical expression (2.34) is of a much simpler form than the exact expression (2.19). In Fig. 1 we present a semilogarithmic plot of the absolute value of the matrix element $p_{\nu\kappa}$ as a function of κ for three different values of ν ($\nu=99=\nu_{\max}80,50$), choosing $\hbar=0.01$. The exact result (2.17) and (2.19) is shown by crosses, and the semiclassical result (2.34) is shown by dots. It can be seen that the exact and semiclassical results are hardly distinguishable; i.e., the agreement is very good. The semiclassical approximation for the matrix elements (after inclusion of our correction for the diverging average density of states) indeed works.

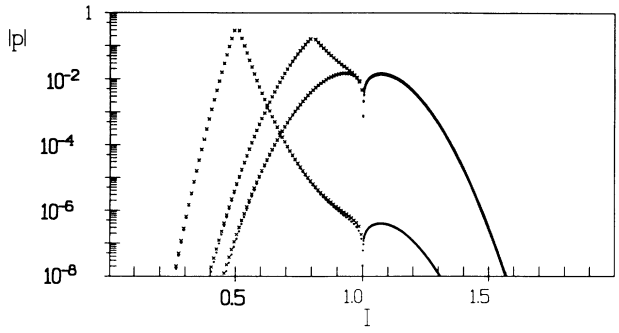

FIG. 1. Discrete-discrete matrix elements $|p|=|p_{\nu\mu}|$ and discrete-continuum matrix elements $|p|=|p_\nu(\kappa)|$ as a function of $I=\hbar(\mu+\frac{1}{2})$ ($I<1$) and $I=1+\hbar\kappa$ ($I>1$) for $\nu=50$ (leftmost peak), $\nu=80$ (middle peak), and $\nu=99$. For $I<1$ the exact results (crosses) and the semiclassical results (dots) are given, but they are hardly distinguishable. For $I>1$ the curves for $\nu=80,99$ practically coincide.

2. *Continuous subspace*

For the unbound motion a pair of canonically conjugate variables I, ϕ analogous to the action angle variables can also be introduced [see I, Eqs. (2.16) and (2.17)] and the molecular Hamiltonian then reads

$$H_0(I) = 1 - I + \tfrac{1}{2}I^2 , \tag{2.35}$$

for $I \geq 1$. Defining $I=1+\hbar\kappa$, we have $H_0=\frac{1}{2}+\frac{1}{2}\hbar^2\kappa^2$. The unbound motion of the momentum $p(I,t)$ is then obtained as

$$p(I,t) = \int_{-\infty}^{+\infty} \frac{d\omega}{2\pi} p(I,\omega) e^{i\omega t} , \tag{2.36}$$

with

$$p(I,\omega) = -2\pi i \cosh\left[\frac{\omega}{I-1}\arccos\left[\frac{-1}{\sqrt{2H_0(I)}}\right]\right] \Big/ \sinh[\pi\omega(I-1)] \tag{2.37}$$

[cf. (2.19) and (2.20) of I].

Applying the symmetrized version of the semiclassical formula for the matrix element analogous to (2.28), we obtain the approximation

$$Np\left[\kappa+\frac{\lambda}{2},\kappa-\frac{\lambda}{2}\right] \approx p(I,\omega) , \tag{2.38}$$

with

$$I = 1+\hbar\kappa , \quad \omega = \hbar\kappa\lambda . \tag{2.39}$$

The normalization factor N is determined from the condition

$$p(I,\omega)\frac{d\omega}{2\pi} = p\left[\kappa+\frac{\lambda}{2},\kappa-\frac{\lambda}{2}\right] d\lambda , \tag{2.40}$$

and hence

$$\frac{d\omega}{2\pi}=\frac{d\lambda}{N}=\frac{\hbar\kappa}{2\pi}d\lambda \ . \tag{2.41}$$

We obtain therefore

$$p(\kappa,\kappa')\approx -i\hbar\left[\frac{\kappa+\kappa'}{2}\right]\cosh\left[(\kappa-\kappa')\arccos\left[\frac{-1}{\sqrt{1+(\hbar^2/4)(\kappa+\kappa')^2}}\right]\right]\Big/\sinh\pi(\kappa-\kappa') \ . \tag{2.42}$$

Correcting for the divergent density of states for $\kappa\to 0$ as in the preceding section by multiplying by the factor $2\sqrt{\kappa\kappa'}/(\kappa+\kappa')$, we obtain finally

$$p(\kappa,\kappa')=-i\hbar\sqrt{\kappa\kappa'}\cosh\left[(\kappa-\kappa')\arccos\left[\frac{-1}{\sqrt{1+\hbar^2(\kappa+\kappa')^2/4}}\right]\right]\Big/\sinh\pi(\kappa-\kappa') \ . \tag{2.43}$$

In Fig. 2 we plot semilogarithmically the absolute value of $|p(\kappa,\kappa')|$ as a function of κ' for three different fixed values of κ ($\kappa=0.125,50,100$), choosing $\hbar=0.01$.

E. Discretization of the continuum

In order to solve (2.15) numerically, we have to discretize the continuum. This can be done by introducing small κ intervals Δ_j centered around discrete values of κ_j which cover the positive κ axis, $j,1,2,\ldots,N_c$. Here N_c is the number of discretized continuum states used in the computation. Introducing the amplitudes

$$y_s=\begin{cases} b_\nu \ , & s=\nu \ , \quad 0\le\nu\le\nu_{\max} \\ \sqrt{\Delta_j}\,b_{\kappa_j} \ , & s=\nu_{\max}+j \ , \quad 1\le j\le N_c \end{cases} \tag{2.44}$$

and, in obvious notation, the matrix elements

$$Z_{sr}=\frac{g}{\omega}\begin{cases} p_{\nu\mu} \\ \sqrt{\Delta_j}\,p_\mu^*(\kappa_j) \\ \sqrt{\Delta_k}\,p_\nu(\kappa_k) \\ \sqrt{\Delta_j\Delta_k}\,p(\kappa_j,\kappa_k) \end{cases} \ , \quad \omega_{sr}=\begin{cases} \omega_{\nu\mu} \\ \omega_{j\mu} \\ \omega_{\nu k} \\ \omega_{jk} \end{cases} \ , \tag{2.45}$$

the Schrödinger equation can be written in the form

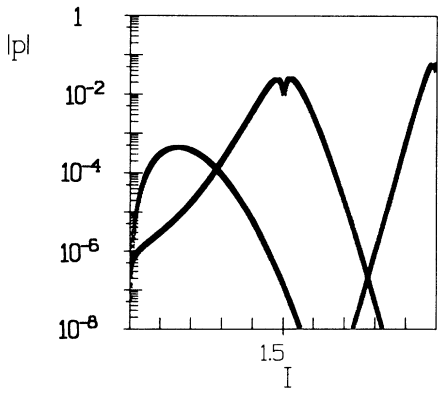

FIG. 2. Continuum-continuum matrix elements $|p|=|p(\kappa,\kappa')|$ in semiclassical approximation as a function of $I=1+\hbar\kappa'$ for $\kappa=0.125$ (leftmost peak), $\kappa=50$ (middle double peak), and $\kappa=100$.

$$i\hbar\dot{y}_s=-\sin\omega t\sum_{r=0}^{\nu_{\max}+N_c}Z_{sr}e^{i\omega_{sr}t}y_r \ . \tag{2.46}$$

In this form the Schrödinger equation can now be soived numerically. The solution will be reliable as long as the time interval is kept small compared with the maximal inverse level spacing introduced in the continuum

$$t\hbar\kappa\min(\Delta_j)\ll 1 \tag{2.47}$$

and as long as the number N_c is sufficiently large to avoid an escape of the state vector from the finite subspace of the Hilbert space considered. If longer times are to be considered, damping terms can be added to (2.46) which are designed to avoid spurious oscillations with the frequencies $\hbar\kappa_j\Delta_j$. Equation (2.46) then reads

$$i\hbar\dot{y}_s=-i\hbar\gamma_s y_s-\sin\omega t\sum_{r=0}^{\nu_{\max}+N_c}Z_{sr}e^{i\omega_{sr}t}y_r \ . \tag{2.48}$$

An obvious choice for the damping rates γ_s is

$$\gamma_s=\begin{cases} 0 \ , & 0\le s\le\nu_{\max} \\ \hbar\kappa_j\Delta_j \ , & \nu_{\max}+1\le s\le\nu_{\max}+N_c \ , \end{cases} \tag{2.49}$$

because these values are the smallest possible if oscillations with the spurious discretization frequencies are still to be damped out.

III. RESULTS AND DISCUSSION

We have solved (2.15) for the parameter values $\omega=1$, $g=0.01$, and $\hbar=0.01$, choosing $N_c=800$ discretized intervals Δ of the continuum of equal size $\Delta=0.125$ in the interval $0\le\kappa\le 100$. In the following various results of these computations are presented.

A. Occupation probabilities of the bound molecular states

Let us first discuss the occupation probability for the bound states of the molecule after it experienced 100 periods of the electromagnetic field, starting in a given bound state with vibrational quantum number ν_0.

In Fig. 3 we show the result for $\nu_0=55$. The solid line gives the occupation probability as a function of the molecular energy for sudden switch-on and switch-off of the field. The dashed line corresponds to a smooth

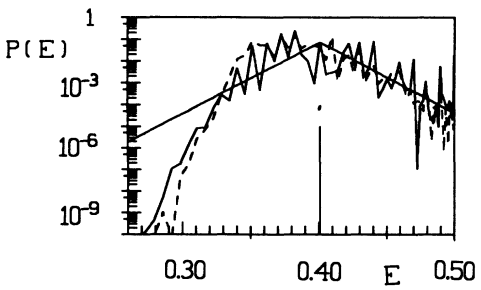

FIG. 3. Occupation probability $P(E)$ of the bound molecular states as a function of E ($0 \le E \le \frac{1}{2}$) after 100 field periods with $\omega = 1.0$, $g = 0.01$ for the initial state $\nu_0 = 55$ (vertical line). Solid line, sudden switch-on and switch-off; dashed line, adiabatic switch-on and switch-off; straight line, mean exponential falloff predicted by localization theory.

switch-on and switch-off during the first and last ten field periods. The switch-on function of the field amplitude which was used has the form $\sin^2(\pi t/20T)$ and similarly for the switch-off. It can be seen that the influence of the smooth switch-on and switch-off is not very large. The same is true for Figs. 4 and 5. The straight line in Fig. 3 gives the exponential fall-off of the occupation probability which follows from the theory for dynamical localization applied to the periodically driven Morse oscillator (see I):

$$P(E) \sim \exp\left[-\frac{2(E-E_0)/\hbar\omega}{l'_A}\right] . \tag{3.1}$$

The localization length l'_A has been calculated in I using the Morse map as

$$l'_A = \frac{1}{4}\frac{2\pi^2 g^2}{(\hbar\omega)^2} e^{-2\omega} . \tag{3.2}$$

We note that l'_A is independent of E and E_0. The slope of the straight line in Fig. 3 (as well as Figs. 4 and 5) was determined from (3.2) and can be seen to give a reasonable description of the overall rate of the exponential falloff. The localization theory thus gives a good description of the occupation probability in the bound subspace for finite excitation times, despite the presence of the continuum. Superimposed on the average exponential falloff are oscillations with maxima separated by the photon energy $\hbar\omega$. This structure is again well explained by the Morse map of I, which predominantly couples states

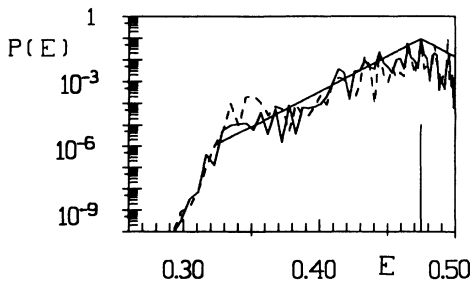

FIG. 4. Same as Fig. 3 for $\nu_0 = 77$.

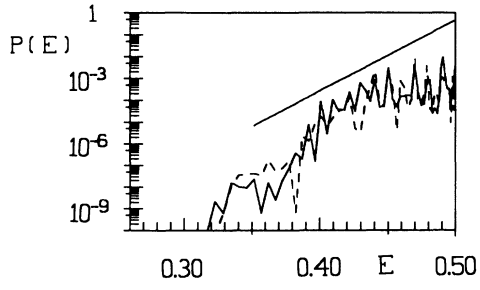

FIG. 5. Same as Fig. 3 for $\nu_0 = 99$.

separated by the photon energy $\hbar\omega$. The energy of the initial states is given as a vertical line in Fig. 3. It is above the energy E_c of the classical chaos border at about $E_c \simeq 0.33$ and below the Cantorus border for quantum dissociation at about $E_Q \simeq 0.41$ (see Fig. 10 of I). The classical chaos border marks the position of the last Kolmogorov-Arnold-Moser (KAM) torus. In Fig. 3 it is seen as the energy where the exponential falloff of the wave function due to dynamical localization goes over into an exponential falloff with a different slope due to quantum tunneling into the classically forbidden domain. On the right-hand side, the energy axis is terminated at the dissociation energy $E = \frac{1}{2}$. Figure 4 gives a similar plot as Fig. 3 with $\nu_0 = 77$. The exponential falloff due to dynamical localization now occurs over a longer distance and is again replaced by tunneling below the energy of the last KAM torus. Finally, in Fig. 5 we have chosen as initial state the last bound state of the molecule with $\nu_0 = 99$. This state most strongly feels the influence of the continuum. The exponential decay with the expected localization length now occurs only at a certain distance from the dissociation energy, which is easily understood as a result of the excitation of the high-lying states into the continuum.

In summary, these results show that adiabatic effects are small for the states we consider and that the localization theory based on the Morse map explains remarkably well the overall form of the excited wave packets in the bound subspace.

B. Energy distribution of dissociated states

We now turn to the occupation probability of the continuum states obtained after 100 field periods, starting with the same bound states as in Sec. III A. In our discussion we shall not consider the further modification of the energy distribution due to ponderomotive effects, which have been frequently discussed and are well understood [17]. In a comparison with experiment, they would, of course, have to be taken into account. In Figs. 6, 7, and 8, we show the results obtained for $\nu_0 = 55$, 77, and 99, respectively.

The results for sudden switch-on and switch-off are shown in Figs. 6(a), 7(a), and 8(a), and those for smooth switch-on and switch-off during the first and last ten field periods are shown in Figs. 6(b), 7(b), and 8(b). In Figs. 6(c), 7(c), and 8(c), we present the result for sudden

switch-on and switch-off by damping the continuum as in (2.48).

Let us first discuss the effect of the smooth switch-on and switch-off. As can be seen from Figs. 6(a) and 6(b), it has a strong quantitative effect on the probability in the continuum for the lowest-lying one among the initial states considered in our examples ($\nu_0=55$). While the form of the energy distribution is similar (in particular, the pronounced peak structure spaced by the photon energy $\hbar\omega$ and the form of the fall-off towards higher energies), the overall size of the occupation probability differs by about an order of magnitude. On the other hand, for the initial states $\nu_0=77$, 99, an appreciable influence of the adiabatic switch-on and switch-off is not present, as can be seen comparing Figs. 7(a) and 7(b) or Figs. 8(a) and 8(b).

Next, we consider Figs. 6(c), 7(c), and 8(c) and discuss the influence of damping the continuum as described in (2.48) and (2.49). It can be seen that it changes the energy distribution in the continuum in a rather strong way, leading to a much more rapid decay of the occupation probability toward higher energies. Numerically, this is, of course, a great advantage, as it allows us, in this case, to work with a smaller subrange of the continuum near the dissociation energy. But to what extent is the more rapid decay in the continuum a physical effect? The answer depends on which aspect of the continuum one is interested in. One may ask, e.g., what is the probability distribution over the continuum, as in Figs. 6–8. The answer is independent of the phase of the wave function in the energy representation and correctly given without damping the continuum. However, one may also ask, e.g., what is the effect of the backaction of the continuum

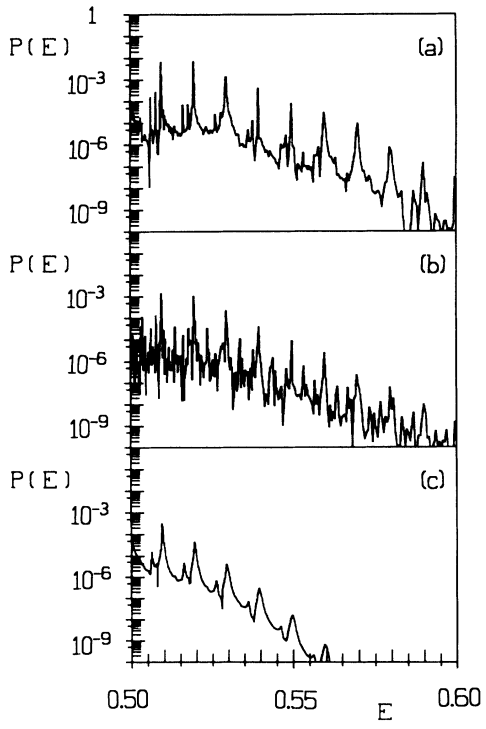

FIG. 6. Occupation probability density of the continuum $P(E)$ as a function of E ($0.5 \le E \le 0.6$) after 100 field periods for the case of Fig. 3 ($\nu_0=55$): (a) for sudden switch-on and switch-off, (b) for smooth switch-on and switch-off, and (c) for the damped continuum.

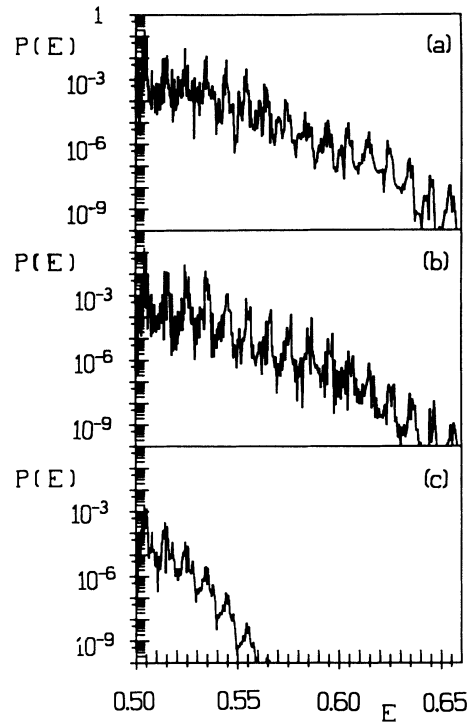

FIG. 7. Same as Fig. 6 for $\nu_0=77$.

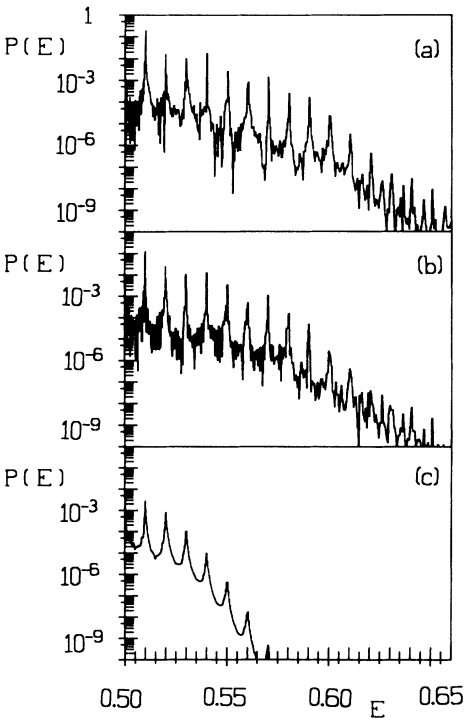

FIG. 8. Same as Fig. 6 for $\nu_0=99$.

on the component of the wave function in the bound subspace shown in Figs. 3–5. The answer to this question depends on the total wave packet, i.e., also on the phase of the wave function in the energy representation. We shall now argue that in this case the damping of the continuum is physical and provides the more accurate description: The discretization of the continuum used for the wave function in our approach in effect replaces the continuum by a quasicontinuum of closely spaced discrete states. Forming this quasicontinuum, we implicitly assume that the amplitudes of all continuum states within a discretization interval add up to the nondecaying amplitude of the discrete state representing that interval in our approximation. Decaying states then only appear as a result of destructive interference between several quasicontinuum states. This assumption is bound to overestimate the size of the probability amplitudes in the quasicontinuum, representing the wave packet. A more physical assumption seems to be that the adding up of the continuum amplitudes within a discretization interval will already lead to a partially decaying amplitude because of a partially destructive interference between closely neighbored continuum states, the decay width being proportional to the size of the discretization interval. This idea immediately leads to (2.48) and (2.49).

Following this reasoning, we have recalculated the occupation probabilities in the bound subspace for the cases of Figs. 3–5 using the damped continuum. The results were found not to differ significantly from those in Figs. 3–5, and they are therefore not recorded here.

Finally, we discuss the overall shape of the energy distribution in the continuum. The most marked feature is the pronounced peak structure spaced by a photon energy $\hbar\omega$, showing that it is not a single-photon process which is responsible for the transition between the bound subspace and continuum. In the description of I using the Morse map, the transition between the bound subspace and continuum occurs when the highly excited, but still bound, molecule during its vibration rapidly passes through the nuclear distance minimum where it very effectively interacts with the electromagnetic field, taking up enough energy for its subsequent dissociation. In the Morse map this is described by a final kick, which the molecule receives before dissociation. In this description the energy distribution over the continuum is therefore determined by the form of the final kick.

According to (4.11) of I, the absolute value of the kick amplitude $K_{E,E'}$ in the energy representation is appreciable only if $E-E'=\hbar\omega(l-l')$, where E',E are the energies before and after dissociation and $(l-l')$ is an integer. It is given by

$$|K_{E,E'}|=\left|J_{l-l'}\left[-\frac{2\pi g}{\hbar\omega}e^{-\omega}\right]\right|, \tag{3.3}$$

where $J_l(x)$ is the Bessel function. Equation (3.3) predicts energies $E=E'+\hbar\omega(l-l')$ of the dissociated state differing by integer multiples of $\hbar\omega$ from the bound-state energy E' before dislocation. Therefore the pronounced peak structure of the bound states, visible in Figs. 3–5, is transferred to the continuum. The peak structure in the continuum is therefore not created by the repeated absorption of single photons, but rather by a single sudden multiphoton event. The overall falloff of $P(E)$ for large E in Figs. 6(a), 6(b), 8(a), and 8(b) can be understood from the asymptotic fall-off of the Bessel function in (3.3) for $|l-l'|>(2\pi g/\hbar\omega)e^{-\omega}$. Taking $E'\simeq 0$ and using l to label the peaks in the continuum, we have

$$|K_{E,O}|^2\sim\frac{1}{2\pi l}\left[\frac{\pi g e^{1-\omega}}{\hbar\omega l}\right]^{2l}, \tag{3.4}$$

which correctly describes the stronger than exponential falloff seen in Figs. 6–8.

The results for the largest energies in Figs. 8(a) and 8(b), and to a lesser extent also in Figs. 7(a) and 7(b), already show some influence of our numerical energy cutoff at $E=1$, but it should be noted that this artifact of the computation occurs only in a region where $P(E)$ is already smaller than 10^{-7}.

C. Dissociation probabilities

The dissociation probability of the molecule is defined by

$$D(t)=1-\sum_{\nu}|b_{\nu}(t)|^2, \tag{3.5}$$

where the sum is taken over the bound states. The results for $D(t)$ for the three initial states $\nu_0=55,77,99$ are shown in Figs. 9(a), 9(b), and 9(c) for sudden switch-on and switch-off (solid line), for smooth switch-on and

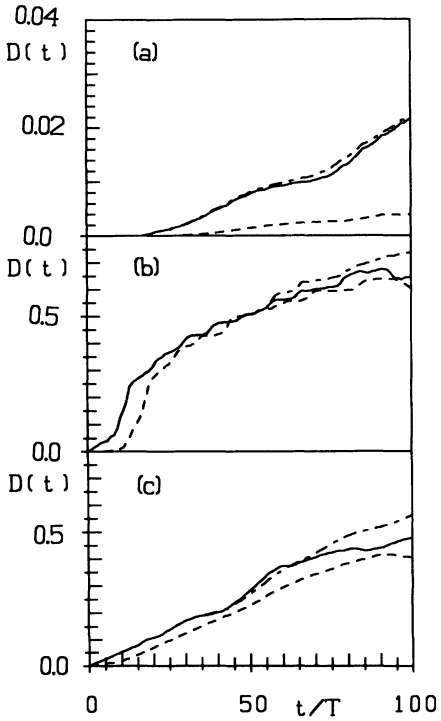

FIG. 9. Dissociation probability $D(t)$ as a function of the number of field periods t/T for sudden switching (solid line), smooth switching (dashed line), and using the damped continuum (dot-dashed line): (a) $\nu_0=55$, (b) $\nu_0=77$, and (c) $\nu_0=99$.

switch-off (dashed line), and for the damped continuum with sudden switch-on and switch-off (dot-dashed line). Only for $\nu_0=55$ is there a strong influence of the smooth switching. In fact, $\nu_0=55$ becomes nearly stable against dissociation for smooth switching. In this context it may be useful to point out the different scales used in Fig. 9(a), 9(b), and 9(c). The near stability of $\nu_0=55$ is consistent with the fact that $\nu_0=55$ was found in I to be below the quantum chaos border formed by the last quantum-mechanically inpenetrable Cantorus, and the appreciable dissociation probability found in I for $\nu_0=55$ (see Fig. 10 of I), for sudden switch-on and switch-off, was hard to explain. It can now be seen to owe its existence only to the high-frequency components contained in the sudden switching. In Figs. 9(b) and 9(c), the dissociation probability $D(t)$ at first rises monotonously in time, as expected, but for $t \geq 80T$ it decreases for short intervals of time in the cases where the undamped continuum is used. This is an artifact which is eliminated by the use of the damped continuum, which, for physical reasons, it is preferable to use in this case (see the discussion in Sec. III B). The use of the undamped quasicontinuum slightly overestimates the feedback from the continuum to the bound subspace. $D(t)$ for $t=100T$ is therefore underestimated in Figs. 9(b) and 9(c), except for the dot-dashed curves.

In Fig. 10 the dissociation probability $D(E)$ after 100 field periods is plotted as a function of the initial energy (diamonds) for sudden switch-on and switch-off and compared with the result obtained in I using the Morse map (solid line). For energies up to $E=0.48$, the agreement is reasonably good, but for energies closer to the dissociation border, the dissociation probability computed by the Morse map is too high. This is probably caused by the increasing difficulty, as the dissociation border is approached, of the conversion from the molecular time scale on which the Morse map is based, which is measured in molecular periods, to the physical time scale, which is measured in field periods (see I). The influence of damping the continuum on Fig. 10 is only slight, as can be seen by the three dots computed for this case.

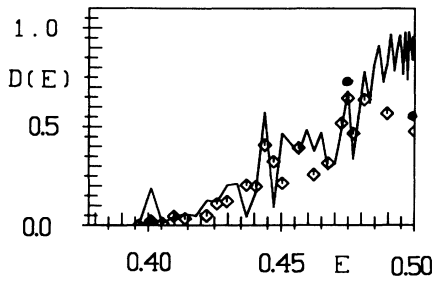

FIG. 10. Dissociation probability D after 100 field periods as a function of the energy $E=\frac{1}{2}-\frac{1}{2}[-\hbar(\nu_0+\frac{1}{2})+1]^2$ of the initial state. The numerical results for sudden switching and undamped continuum (diamonds) are compared with the prediction of the Morse map (solid line). The influence of damping the continuum (dots) is shown for $\nu_0=55,77,99$.

ACKNOWLEDGMENTS

We would like to thank Dima Shepelyansky for suggesting the exploration of the influence of damping the continuum. This work was supported by the "Deutsche Forschungsgemeinschaft" through the "Sonderforschungsbereich 237." The numerical work was carried out at the HLRZ in Juelich.

APPENDIX A

Here we wish to present the calculation of the matrix elements

$$x_\nu(\kappa)=\int_{-\infty}^{+\infty} dx\, \phi_\nu^*(x)x\phi(x,\kappa)\ . \tag{A1}$$

Inserting the eigenfunctions (2.4) and (2.8) and the substitution (2.5), (A1) is given by the integral

$$x_\nu(x)=-\frac{N_\nu N(\kappa)}{2^{\beta_\nu+i\kappa}}J_\nu(\kappa)\ , \tag{A2}$$

with

$$\begin{aligned} J_\nu(\kappa)&=\int_0^\infty dz\, z^{\beta+i\kappa-1}e^{-z}(\ln z)L_\nu^{(2\beta)}(z) \\ &\quad\times U(i\kappa+\tfrac{1}{2}-\gamma,2i\kappa+1,z)\ , \\ \gamma&=\hbar^{-1}\ ,\quad \beta=\beta_\nu=\gamma-(\nu+\tfrac{1}{2})\ , \\ N_\nu&=2^\beta[2\beta n!/\Gamma(\nu+2\beta+1)]\ , \end{aligned} \tag{A3}$$

and $N(\kappa)$ given by (2.11). Expressing $L_\nu^{(2\beta)}(z)$ and $U(i\kappa+\frac{1}{2}-\gamma,2i\kappa+1,z)$ in terms of Whittaker's functions $M_{\gamma,\beta}(z)$ and $M_{\gamma,i\kappa}(z), M_{\gamma,-i\kappa}(z)$, respectively, by means of standard relations [12] and using the relation $z^y\ln z=(dz^{x+y}/dx)_{x=0}$, the integral $J_\nu(\kappa)$ can be written as

$$\begin{aligned} J_\nu(\kappa)&=\mathrm{Re}\left[\frac{dJ_\nu(x,\kappa)}{dx}\right]_{x=0}\ , \\ J_\nu(x,\kappa)&=2\begin{bmatrix}\nu+2\beta\\ \nu\end{bmatrix}\frac{\Gamma(-2i\kappa)}{\Gamma(\frac{1}{2}-2i\kappa-\gamma)}I(x,\kappa)\ , \end{aligned} \tag{A4}$$

where $I(x,\kappa)$ is the integral

$$I(x,\kappa)=\int_0^\infty dz\, z^{x-2}M_{\gamma,\beta}(z)M_{\gamma,i\kappa}(z)\ . \tag{A5}$$

It can be evaluated and the derivative of x taken. Using the ψ function defined by

$$\frac{d\Gamma(x)}{dx}=\psi(x)\Gamma(x)\ , \tag{A6}$$

we obtain

$$\left[\frac{dI(x,\kappa)}{dx}\right]_{x=0}=\frac{\Gamma(1+2i\kappa)}{\Gamma(i\kappa+\frac{1}{2}+\gamma)}\sum_{l=0}^{\infty}\frac{(-n)_l\Gamma(\beta+i\kappa+l)\Gamma(\nu+1-l)}{l!(1+2\beta)_l\Gamma(i\kappa-\beta-l+1)}[\psi(\beta+i\kappa+l)-\psi(\nu+1-l)+\psi(i\kappa-\beta-l+1)]. \tag{A7}$$

Further simplification is achieved by using the identities

$$(-\nu)_l\Gamma(\nu+1-l)=(-1)^l\nu!\ ,\quad \Gamma(i\kappa-\beta-l+1)=\frac{(-1)^l\Gamma(i\kappa-\beta+1)}{(\beta-i\kappa)_l}\ . \tag{A8}$$

Combining the resulting expression for (A7) with (A4), we obtain

$$J_\nu(\kappa)=2\mathrm{Re}\left[\begin{pmatrix}\nu+2\beta\\ \nu\end{pmatrix}\frac{\nu!\Gamma(1+2i\kappa)\Gamma(-2i\kappa)S(\nu,\kappa)}{\Gamma(\frac{1}{2}-i\kappa-\gamma)\Gamma(\frac{1}{2}+i\kappa+\gamma)\Gamma(1+i\kappa-\beta)\Gamma(\beta-i\kappa)}\right]\ , \tag{A9}$$

with

$$S(\nu,\kappa)=\sum_{l=0}^{\nu}\frac{|\Gamma(\beta+i\kappa+l)|^2}{l!(1+2\beta)_l}[\psi(\beta+i\kappa+l)-\psi(\nu+1-l)+\psi(i\kappa-\beta-l+1)]\ . \tag{A10}$$

Equation (A9) may be simplified using the relations

$$\begin{aligned}&\Gamma(1+2i\kappa)\Gamma(-2i\kappa)=\frac{i\pi}{\sinh 2\pi\kappa}\ ,\\ &\Gamma(1+i\kappa-\beta)\Gamma(\beta-i\kappa)=\frac{\pi}{\beta-i\kappa}\ ,\\ &\Gamma(\tfrac{1}{2}+\gamma+i\kappa)\Gamma(\tfrac{1}{2}-\gamma-i\kappa)=\frac{\pi}{\sin\pi(\frac{1}{2}+\gamma+i\kappa)}\ .\end{aligned} \tag{A11}$$

In the last of these relations, we may use (2.5) to rewrite

$$\sin\pi(\tfrac{1}{2}+\gamma+i\kappa)=(-1)^{\nu+1}\sin\pi(\beta+i\kappa)\ . \tag{A12}$$

Equation (A9) is then reduced to

$$J_\nu(\kappa)=2\begin{pmatrix}\nu+2\beta\\ \nu\end{pmatrix}\frac{\nu!(-1)^\nu|\sin\pi(\beta+i\kappa)|^2}{\pi\sinh 2\pi\kappa}\mathrm{Im}S(\nu,\kappa)\ . \tag{A13}$$

The imaginary part of (A10) can be evaluated using the relation

$$\psi(z)-\psi(1-z)=-\pi\cot\pi z\ , \tag{A14}$$

which implies

$$\mathrm{Im}[\psi(\beta+i\kappa+l)-\psi(\nu+1-l)+\psi(i\kappa-\beta-l+1)]=\frac{\pi}{2}\frac{\sinh 2\pi\kappa}{|\sin\pi(\beta+i\kappa)|^2}\ , \tag{A15}$$

independent of l.

Hence we arrive at

$$\mathrm{Im}S(\nu,\kappa)=\frac{\pi}{2}\frac{\sinh 2\pi\kappa\Gamma(1+2\beta)}{|\sin\pi(\beta+i\kappa)|^2}\sum_{\lambda=0}^{\nu}\frac{|\Gamma(\beta+i\kappa+\lambda)|^2}{\lambda!\Gamma(1+2\beta+\lambda)}\ . \tag{A16}$$

Combining (A16) with (A13), inserting the result for $J_\nu(\kappa)$ in (A2), and using the prefactors (A3) and (2.11), we obtain the result given in (2.21). The desired matrix element is thereby expressed by a finite sum.

Using an identity given in [15], which we shall prove in Appendix B, this finite sum can, in fact, also be evaluated, and we obtain the closed-form expression given in (2.23).

APPENDIX B

Here we wish to prove the identity

$$F(z)=G(z)\ , \tag{B1}$$

between the two functions F and G, defined by

$$\begin{aligned}F(z)&=\frac{m!\Gamma(k-m)}{\Gamma(m+z+1)\Gamma(k-m-z)}\\ &\quad\times\sum_{j=0}^{m}\frac{\Gamma(j+z)\Gamma(j+k-2m-1-z)}{j!\Gamma(k+j-2m)}\ ,\\ G(z)&=-\frac{1}{z(z+1+2m-k)}\ ,\end{aligned} \tag{B2}$$

if k is not integer; m will be assumed to be an integer, $m\geq 0$. For real $z>0$ the identity was stated without proof in (2.4) of Ref. [15]. As we wish to make use of this identity for complex z in order to evaluate the sum in (2.21) and are not aware of a published proof, we shall here supply one. To this end we observe the following.

(i) For $m=0$ and 1, the identity is easily checked. So we can assume $m\geq 2$ in the following.

(ii) $F(z)$ and $G(z)$ are both analytic functions of z except for simple poles and satisfy

$$\lim_{|z|\to\infty}F(z)=0=\lim_{|z|\to\infty}G(z)\ . \tag{B3}$$

(iii) $F(z)$ may have simple poles (if, as we assumed, k is not integer) at

$$\begin{aligned}&z=z_p=-p\ ,\quad 0\leq p\leq m\quad (p\text{ integer})\ ,\\ &z=\tilde{z}_q=k-2m-1+q\ ,\quad 0\leq q\leq m-2\quad (q\text{ integer})\ .\end{aligned} \tag{B4}$$

(iv) $G(z)$ has simple poles at

$$\begin{aligned}&z=z_0=0\ ,\\ &z=\tilde{z}_0=k-2m-1\ ,\end{aligned} \tag{B5}$$

with residues

$$\mathrm{Res}G(z_0)=\mathrm{Res}G(\tilde{z}_0)=-\frac{1}{1+2m-k}\ . \tag{B6}$$

In order to prove the identity (B1), it merely remains to show that

$$\mathrm{Res}F(z_0)=\mathrm{Res}F(\tilde{z}_0)=-\frac{1}{1+2m-k}\ , \tag{B7}$$

$$\mathrm{Res}F(z_p)=\mathrm{Res}F(\tilde{z}_q)=0\ ,$$

$$m\geq p\geq 1\ ,\quad m-2\geq q\geq 1\ . \tag{B8}$$

The residues of F at the poles z_0 and $\tilde{z}_0$ are easily evaluated from the definition (B2). Only the terms of the sum for $j=0$ contribute in both cases. Equation (B7) is there-

by easily established. Let us now evaluate, for $p \geq 1$,

$$\begin{aligned}\mathrm{Res}F(z_p) &= \lim_{x\to 0} xF(x-p) \\ &= \lim_{x\to 0} \sum_{j=0}^{m} \frac{x\Gamma(x-p+j)\Gamma(j+k-2m+p-1)}{j!\Gamma(k+j-2m)} \\ &= \left[\left(\frac{\partial}{\partial y}\right)^{p-1} \sum_{j=0}^{p} \frac{(-1)^{j-p}}{j!(p-j)!} y^{j+k-2m+p-2}\right]_{y=1} \\ &= \left[\left(\frac{\partial}{\partial y}\right)^{p-1} y^{k-2m+p-2}(-1)^p(1-y)^p\right]_{y=1} = 0 \, . \end{aligned} \tag{B9}$$

Similarly, we evaluate, for $q \geq 1$,

$$\mathrm{Res}F(\bar{z}_q) = \lim_{x\to 0} xF(x+k-2m-1+q) = 0 \, . \tag{B10}$$

As the steps of the calculation are very similar to those given in (B9), there is no need to record them here. The identity (B1) is thereby proven for k not an integer. For k an integer it follows by analytical continuation in k. The sum defining $F(z)$ in (B2) can be identified with the sum appearing in (2.21) by identifying $m=\nu$, $k=2/\hbar$, $z=\beta_\nu+i\kappa$, and $j=\lambda$.

[1] M. E. Goggin and P. W. Milonni, Phys. Rev. A **37**, 796 (1988).

[2] J. J. Tanner and M. Matti Maricq, Phys. Rev. A **40**, 4054 (1989).

[3] T. M. Flosnik and R. E. Wyatt, Phys. Rev. A **40**, 5716 (1989).

[4] R. Graham and M. Höhnerbach, Phys. Rev. Lett. **64**, 637 (1990).

[5] P. A. Dando and D. Richards, J. Phys. B **23**, 3179 (1990).

[6] F. Bensch, H. J. Korsch, and N. Moiseyev, J. Phys. B **24**, 1321 (1991).

[7] R. Graham and M. Höhnerbach, Phys. Rev. A **43**, 3966 (1991).

[8] G. Casati and L. Molinari, Prog. Theor. Phys. Suppl. **98**, 287 (1989).

[9] G. Casati, I. Guarneri, and D. L. Shepelyansky, IEEE J. Quantum Electron. **24**, 1420 (1988).

[10] S. M. Susskind and R. V. Jensen, Phys. Rev. A **38**, 711 (1988).

[11] J. Rundgren, Ark. Fys. **30**, 61 (1965).

[12] *Handbook of Mathematical Functions,* edited by M. Abramowitz and I. A. Stegun (Dover, New York, 1965).

[13] P. Eckelt and H.-J. Korsch, Chem. Phys. Lett. **18**, 584 (1973).

[14] R. Graham, Phys. Rev. A **25**, 3234 (1982).

[15] J. A. C. Gallas, Phys. Rev. A **21**, 1829 (1980).

[16] L. D. Landau and E. M. Lifschitz, *Quantenmechanik* (Akademie Verlag, Berlin, 1965).

[17] H. G. Muller, A. Tip, and M. J. van der Wiel, J. Phys. B **16**, L679 (1983); M. H. Mittelman, *ibid.* **17**, L351 (1984); A.Szöke, *ibid.* **18**, L427 (1985); H. G. Muller and A. Tip, Phys. Rev. A **30**, 3039 (1984); S. I. Chu and J. Cooper, *ibid.* **32**, 2769 (1985); J. Javanaienen, J. H. Eberly, and Qichang Su, *ibid.* **38**, 3430 (1988).